Catalysis Letters Vol. 110, Nos. 1–2, August 2006 (© 2006)
DOI: 10.1007/s10562-006-0100-4

A kinetic and DRIFTS study of supported Pt catalysts for NO oxidation

Yaying Ji,[a] Todd J. Toops,[b] Uschi M. Graham,[a] Gary Jacobs,[a] and Mark Crocker[a,*]

[a]*Center for Applied Energy Research, University of Kentucky, 2540, Research Park Drive, Lexington, KY 40511, USA*
[b]*Fuels, Engines and Emissions Research Center, Oak Ridge National Laboratory, 2360, Cherahala Blvd., Knoxville, TN 37932-1563, USA*

Received 8 March 2006; accepted 23 May 2006

NO oxidation was studied over Pt/CeO_2 and Pt/SiO_2 catalysts. Apparent activation energies (E_a) of 31.4 and 40.6 kJ/mole were determined for Pt/CeO_2 and Pt/SiO_2, respectively, while reaction orders for NO and O_2 were fractional and positive for both catalysts. Pre-treatment of the catalysts with SO_2 caused a decrease in the E_a values, while the reaction orders were only slightly changed. *In situ* DRIFTS measurements indicated that high concentrations of nitrate species were formed on the surface of Pt/CeO_2 during NO oxidation, while almost no surface species could be detected on Pt/SiO_2. The addition of SO_2 resulted in the formation of a highly stable sulfate at the expense of nitrate species and caused an irreversible loss of catalytic activity for Pt/CeO_2.

KEY WORDS: nitric oxide; oxidation; platinum; ceria; silica.

1. Introduction

The oxidation of NO to NO_2 over supported Pt catalysts plays a key role in a number of environmental processes, including NO_x abatement using NO_x storage-reduction (NSR) catalysts [1], the selective catalytic reduction (SCR) of NO_x using ammonia as the reductant [2], and the oxidation of soot in catalyzed diesel particulate filters (DPFs) [3]. While Pt is the metal of choice due to its unparalleled activity, the nature of the support material and the Pt dispersion also significantly affect catalyst performance. Studies comparing the properties of Pt on different supports show a clear trend with respect to catalyst activity in NO oxidation,$SiO_2Al_2O_3ZrO_2$ [4–6]. This ordering can be rationalized on the basis that NO is adsorbed principally on the support and then migrates to Pt where it is oxidized [5]. Given that NO is weakly adsorbed on silica, and that NO_2 is not stored as nitrates, the use of silica as support favors rapid migration of adsorbed NO to Pt, followed by oxidation and facile desorption of NO_2. A complicating factor is the dispersion of the supported Pt. Several studies have shown that the rate of NO oxidation on Pt/SiO_2 [4,5,7] and Pt/Al_2O_3 [5,8,9] shows a marked particle size dependency, larger Pt particles exhibiting higher specific activity than smaller ones. Hence, catalyst activity for NO oxidation is likely to be a function of both these effects.

To date the majority of kinetic and mechanistic studies have focused on Pt/Al_2O_3, $Pt/BaO/Al_2O_3$ and Pt/SiO_2 catalysts [4–17], based on their potential use in automotive applications. In contrast, there have been few reports concerning the properties of Pt supported on CeO_2. This is somewhat surprising, given that CeO_2 and$CeO_2 - ZrO_2$ mixed oxides, along with Pt, are widely used as washcoat components in catalyzed particulate filters [18] and NSR catalysts for lean-burn gasoline engines [19]. In the latter case, the role of the ceria component is principally to provide the necessary oxygen storage capacity when the engine is operating at the stoichiometric point (i.e., the catalyst is functioning as a conventional three-way catalyst), although it also promotes H_2 formation under rich conditions via the water–gas shift reaction [20], as well as providing additional NO_x storage capacity during lean operation. Indeed, several recent studies have shown that CeO_2 and$CeO_2 - ZrO_2$ provide excellent NO_x storage at low temperatures [21,22]. Hence for both DPF and NSR applications, Pt supported on CeO_2 or$CeO_2 - ZrO_2$ can be anticipated to play a significant role in NO oxidation.

In this context, current understanding of the properties of$Pt/CeO_2 - ZrO_2$ is confined to a study by Djéga-Mariadassou and co-workers [17], concerning the steady state kinetics of NO oxidation on $Pt/Ce_{0.25}Zr_{0.75}O_2$ and Pt/SiO_2. For both catalysts reaction orders in NO and O_2 were found to be fractional and positive, from which a sequence of elementary steps and a detailed rate equation were proposed. Additionally, as part of a study of supported Pt catalysts for NO sensor applications [5], the activity of Pt/CeO_2 in NO oxidation has recently been examined. Based on turnover frequencies at 200 °C (for catalysts with similar Pt dispersions), Pt/CeO_2 was found to be more active than Pt supported on TiO_2, ZrO_2, Y_2O_3-stabilized ZrO_2 or$Al_2O_3 - SiO_2$, although less active than Pt/SiO_2 and Pt/Al_2O_3.

The paucity of data concerning the kinetics and mechanism of NO oxidation over Pt/CeO_2 prompted us to undertake the current study. In addition to examining

*To whom correspondence should be addressed.
E-mail: crocker@caer.uky.edu

the steady state kinetics of the NO + O_2 reaction over Pt/CeO_2, DRIFTS measurements were performed in order to probe the mechanism of NO oxidation. For comparison purposes Pt/silica was included in the study, as an example of a system in which the support shows minimal capacity for NO_x storage.

2. Experimental

2.1. Catalyst preparation

Two catalyst supports were employed in this study: a commercial silica (Davison Catalysts, BET surface area of 320 m^2/g) and ceria (BET surface area of 74 m^2/g) prepared by precipitation from aqueous cerium nitrate using ammonium hydroxide as the precipitating agent. The cerium hydroxide precipitate was subsequently calcined at 400 °C in air for 4 h. Supported Pt catalysts were prepared by incipient wetness impregnation with aqueous $Pt(NH_3)_4(NO_3)_2$, the target Pt loading being 0.5 wt%. After standing at room temperature overnight, impregnated samples were dried on a rotary evaporator at 60 °C and then calcined in air at 500 °C for 2 h.

2.2. Catalyst characterization

BET surface area and pore volume measurements were performed by nitrogen adsorption at −196 °C using a Micromeritics Tri-Star 3000 system. Catalyst samples were outgassed overnight at 160 °C under vacuum prior to the measurements. The Pt loading was determined by X-ray fluorescence spectroscopy (XRF). Sulfur contents were determined by combustion analysis using a LECO SC-432 analyzer. Pt dispersion measurements for Pt/SiO_2 were performed by hydrogen chemisorption using a Zeton-Altamira AMI-200 unit, equipped with a thermal conductivity detector (TCD). Samples were pre-treated in a H_2/Ar flow at 400 °C for 1 h and then cooled under flowing H_2/Ar to 50 °C. Temperature programmed desorption (TPD) was subsequently carried out in flowing Ar from 50 to 400 °C at a ramp rate of 10 °C/min. The total amount of hydrogen chemisorbed on Pt was obtained from the TPD profile, and the Pt dispersion was calculated on the assumption of a 1:1 H:Pt stoichiometric ratio and a spherical particle morphology. HR-TEM images were acquired using a JEOL 2010-F FasTEM Field Emission Electron Microscope, operated at 200 kV. The point-to-point resolution was 0.2 nm. A minimum contrast technique was used to enhance the visibility of the Pt nanoparticles on the silica and ceria supports.

2.3. Kinetic study

Kinetic measurements were performed in a stainless steel reactor with an internal diameter of 10 mm, contained in a vertical tubular furnace. The feed gas contained 250 ppm NO, 3.5% O_2, 0 or 3.5% H_2O and N_2 as the balance. The total gas flow rate was 1667 $cm^3\ min^{-1}$. Water was added to the feed by means of a syringe pump via a steam generator and heated gas lines maintained at 140 °C. Glass beads were placed upstream of the catalyst to ensure adequate mixing and uniformity of the gas flow. Prior to performing the kinetic measurements, a series of experiments using catalysts of different particle size were performed in order to check that NO conversion was subject to chemical control only. A sieve fraction of 106–180 μm was found to be sufficiently small to exclude mass transfer limitations. In order to operate the reactor in a differential manner, 0.15 g of Pt/SiO_2 and 0.62 g of Pt/CeO_2 were used, the NO conversion being restricted to no more than 15%. At the end of each kinetic run, the conditions of the first data point were duplicated to check for possible catalyst deactivation. For the determination of apparent activation energies, the temperature was varied in a non-sequential manner in order to avoid systematic errors. Similarly, when testing the effect of gas composition on the rate, the concentration of the species of interest was varied non-sequentially, while the concentrations of the other species were kept constant.

2.4. DRIFTS study

DRIFTS measurements were performed in an integrated stainless-steel reaction cell, using a MIDAC model M2500 FTIR spectrometer coupled with a Harrick Scientific barrel ellipsoidal mirror DRIFT accessory. The system is typically operated at slightly below atmospheric pressure (around 500 Torr) to prevent stagnation in the cell and to maintain the seal between the removable hemispherical ZnSe dome and the cell body. Tylan General mass flow controllers were used to establish the inlet gas concentrations, in conjunction with a sparger system submerged in a NESLAB RTE-110 recirculating constant temperature bath that controlled the inlet concentration of H_2O.

The catalysts were first pretreated in flowing Ar at 450 °C for 30 min and then allowed to cool to 25 °C. For the TPD experiments the catalysts were exposed to the flowing feed gas at 25 °C, DRIFTS spectra being recorded as a function of time. Subsequently, the gas flow was changed to Ar, the sample was heated and further spectra recorded at regular temperature intervals. Additionally, *in situ* DRIFTS measurements were made during NO oxidation, using a flowing gas mixture of 500 ppm NO and 5.0% O_2 in Ar.

3. Results and discussion

3.1. Kinetic study

NO oxidation was initially performed in the absence of H_2O, CO_2 and SO_2. Figure 1(a) shows the temperature dependence of the NO oxidation rate for the two catalysts

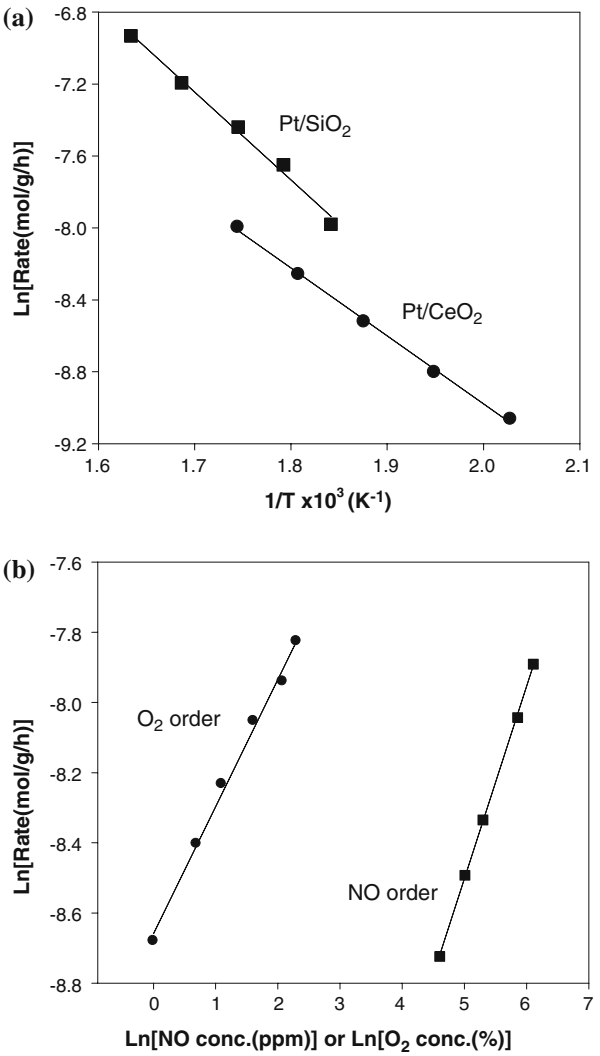

Figure 1. (a) Arrhenius plots of NO oxidation over Pt/CeO_2 and Pt/SiO_2; feed: 250 ppm NO, 3.5% O_2. (b) NO and O_2 concentration dependence of NO oxidation rate over Pt/CeO_2 at 280 °C; feed for NO order determination: 100–450 ppm NO, 3.5 % O_2; feed for O_2 order determination: 250 ppm NO, 1–10% O_2.

in the range 220–340 °C, the rate being defined as moles of NO reacted per hour per gram of catalyst. Pt/SiO_2 exhibited a higher reaction rate than Pt/CeO_2, consistent with results reported by Bernard *et al.* [5]. Table 1 shows that the apparent activation energy (E_a) determined for the Pt/SiO_2 catalyst is 40.6 kJ/mole, which is less than the value of 57.7 kJ/mole reported by Marques *et al.* [17]. This difference may be due to the different chemical state of the Pt in the catalysts studied. In the present work, Pt should be mainly present in an oxidic state, given the small size of the supported Pt particles (Pt dispersion of 0.80) and that no reduction step was applied; this contrasts with the reduced catalyst studied by Marques *et al.* which possessed a lower Pt dispersion of 0.21. Relative to Pt/SiO_2, Pt/CeO_2 possesses a slightly lower E_a of 31.4 kJ/mole, this being similar to the E_a value of 34.6 kJ/mole reported for $Pt/CeZrO_2$ [17].

To determine the reaction orders in NO and O_2, their concentrations were independently varied over the ranges 100–450 ppm NO and 1–10% O_2 (Figure 1(b)). In the case of Pt/SiO_2, the reaction orders in NO and O_2 were found to be 0.46 and 0.52, respectively, while those determined for Pt/CeO_2 were 0.55 and 0.36 (Table 1). These reaction orders are similar to those reported by Marques *et al.* [17] for Pt/SiO_2 and $Pt/CeZrO_2$ at 217 and 308 °C, respectively. The effect of CO_2 and H_2O on NO oxidation kinetics was also examined. In the case of CO_2, no influence on the oxidation rate was found for either catalyst at an added CO_2 concentration of 12%. The addition of water (3.5%) to the feed also had no discernable effect on NO oxidation over Pt/SiO_2, although it resulted in a marked decline in the catalytic activity of Pt/CeO_2, NO conversion decreasing from 14.3% to 10.6% at 280 °C. Concomitantly, the apparent activation energy increased from 31.4 to 36.9 kJ/mole, while there was almost no influence on the reaction orders in NO and O_2. The basis of this inhibition will be discussed in Section 3.2.4.

Catalyst deactivation due to poisoning by SO_2 is a ubiquitous problem in emission control catalysis. In a previous study, we found that NO oxidation catalysts based on transition metal oxides were severely deactivated in the presence of high SO_2 concentrations [23]. Under the reaction conditions used in this study, the addition of only 100 ppm SO_2 was found to suppress the steady state NO conversion to such low levels that

Table 1
Summary of kinetic parameters for NO oxidation over Pt catalysts

Catalyst	Reaction condition	E_a (kJ/mol)[a]	NO order[b,d]	O_2 order[c,d]
Pt/SiO_2	$NO + O_2$	40.6	0.46	0.52
	$NO + O_2$ (SO_2-exposed)	32.5	0.37	0.51
Pt/CeO_2	$NO + O_2$	31.4	0.55	0.36
	$NO + O_2 + H_2O$	36.9	0.49	0.33
	$NO + O_2$(SO_2-exposed)	24.2	0.57	0.42

[a]Feed gas: 250 ppm NO, 3.5% O_2, 3.5% H_2O where indicated, N_2 as balance.
[b]Feed gas: 3.5% O_2, 100–450 ppm NO, N_2 as balance.
[c]Feed gas: 250 ppm NO, 1–10% O_2, N_2 as balance.
[d]Reaction order determined at 300 °C for Pt/SiO_2 and 280 °C for Pt/CeO_2.

accurate kinetic measurements became difficult. Although catalyst deactivation is much more gradual at low SO_2 concentrations (e.g., a few ppm), it is difficult to ascertain when (and if) the catalyst has reached a steady state. Therefore, we chose to study NO oxidation in the absence of SO_2, over catalysts which had previously been poisoned by exposure to SO_2. In each case the catalyst was first exposed to a mixture containing NO, O_2 and 100 ppm SO_2 at 300 °C. SO_2 addition was ceased after the NO conversion had dropped to ~25% of the original value (< 30 s). After this, the catalyst was allowed to equilibrate in the $NO + O_2$ mixture at 300 °C for a prolonged period until a steady state was reached. Subsequently, kinetic measurements were performed on the sulfated catalyst (in the absence of H_2O and CO_2). In agreement with previous results [6], the activity of Pt/SiO_2 is largely restored after removal of SO_2 from the feed. In contrast, Pt/CeO_2 exhibited only a slight recovery in NO conversion. The resulting kinetic data are collected in Table 1. In both cases, the catalyst exposed to SO_2 showed a lower apparent activation energy as compared to the fresh catalyst, while the reaction orders in NO and O_2 were only slightly changed. These changes in E_a are accompanied by changes in the physical properties of the catalysts. As shown in Table 2, hydrogen chemisorption revealed an increase in mean Pt particle size from 1.5 to 3.3 nm for Pt/SiO_2, while the BET surface area and pore volume were essentially unaffected. Additionally, a residual sulfur content of 0.15 wt% was measured. In contrast, the surface area of the Pt/CeO_2 catalyst showed a marked decrease from 68.8 to 36.3 m^2/g, while the average pore radius increased from 6.2 to 8.9 nm. These observations, combined with the measured residual sulfur content of 1.7 wt%, are consistent with sulfation of the ceria support as described in the DRIFTS study below.

High resolution TEM imaging was applied to obtain information on the size, morphology and distribution of Pt nanoclusters in the catalyst samples. For the as-prepared Pt/SiO_2 catalyst (figure 2), the majority of the Pt nanoparticles are around 2 nm in diameter and are characterized by a semi-spherical morphology. Larger particles with diameters ranging up to 15 nm can also be occasionally observed, corresponding to agglomerates of smaller particles. The Pt/SiO_2 sample exposed to SO_2 is shown in figure 2(c) and contains another type of Pt nanoparticles, which are significantly larger compared with the 2–15 nm Pt particles. The second type forms semi-rectangular grains as seen in figure 2(c), the size of which was found to range up to 35 nm in length and up to 25 nm in width. These particles occur infrequently and in a random orientation throughout the micron-sized SiO_2-clusters. Overall these observations are consistent with the hydrogen chemisorption data, which show a growth in the average Pt particle size after SO_2 exposure. In this context, we note that there are several reports in the literature of Pt particle sintering occurring as a consequence of exposure to sulfur compounds [24,25]. The fact that the increase in Pt particle size has only a small effect on the reaction rate is associated with the finding that the specific activity for NO oxidation increases with increasing particle size [4,5,7]. That the rate does not increase suggests that this higher specific activity is balanced by the lower number of surface Pt

Table 2
Physical properties of the catalysts as-prepared and after sulfation

Catalyst	Metal (wt%)	Condition	Sulfur (wt%)	BET SA (m^2/g)	Vp (cm^3/g)	Mean pore radius (nm)	Pt dispersion[a]	Pt particle size from TEM (nm)
Pt/SiO_2	0.57	As prepared	–	295.7	1.208	7.7	0.80	2–15
		After sulfation	0.15	293.6	1.200	7.7	0.36	2–35
Pt/CeO_2	0.44	As prepared	–	68.8	0.212	6.2	–	0.5–2.0
		After sulfation	1.70	36.3	0.180	8.9	–	0.5–2.5

[a] Determined by H_2 chemisorption.

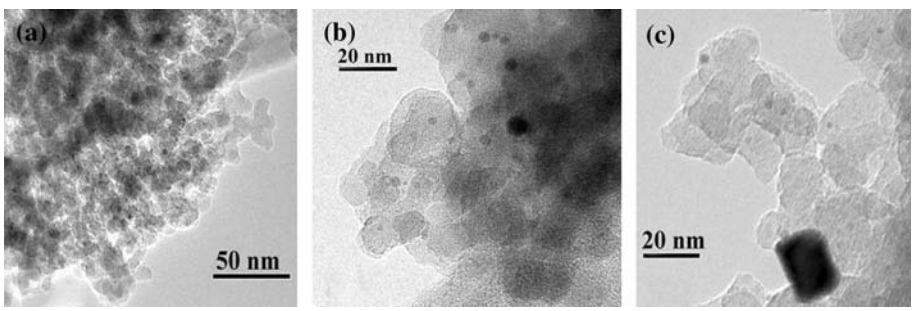

Figure 2. TEM images of Pt/SiO_2: (a) as-prepared (low resolution), (b) as-prepared sample (high resolution), (c) SO_2-exposed.

sites, and possibly that some surface sites may be poisoned by residual sulfur.

The Pt/CeO_2 catalyst is illustrated in figure 3. Unlike the semi-spherical Pt nanoparticles hosted by the amorphous SiO_2 support which were easily recognized in TEM, the ones supported on the CeO_2 crystal surfaces are more difficult to image. This is in part caused by the interaction of the heavier cerium atoms with the electron beam, as compared to the silicon atoms, although it may also be caused by the denser crystal surfaces. The HRTEM images in figure 3(b) and (c) reveal the Pt nanoparticles for the as-prepared and SO_2-exposed samples, the particles in both cases being semi-rectangular in shape. It is not clear whether the crystalline nature of the support controls the morphology and smaller size of the Pt nanoparticles, which have a narrow size range of 0.5–2.5 nm. While meaningful Pt dispersions could not be determined from the TEM data (due to the difficulty of imaging the particles), comparison of the Pt nanoparticles on the CeO_2 crystal surfaces of the two samples suggests that sintering of the Pt particles in the SO_2-exposed sample is minor.

3.2. DRIFTS measurements

3.2.1. Adsorption of NO and NO_2

After adsorbing NO at room temperature, DRIFT spectra were recorded as a function of temperature in flowing Ar. As shown in figure 4(a), the appearance of broad, disproportionate bands coincided with the introduction of NO on Pt/CeO_2 at 25 °C, indicating the presence of several types of adsorbed species. A strong band at 1187 cm^{-1} can be assigned to chelating nitrite, as can a weaker band at 1295 cm^{-1} [26]. Bands at 1602

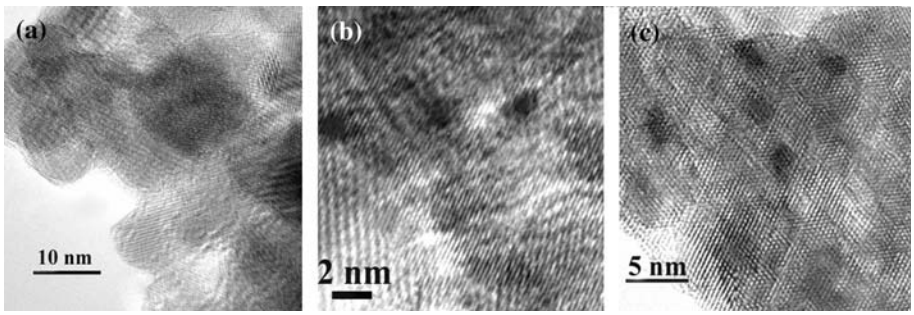

Figure 3. TEM images of Pt/CeO_2: (a) as-prepared (low resolution), (b) as-prepared sample (high resolution), (c) SO_2-exposed.

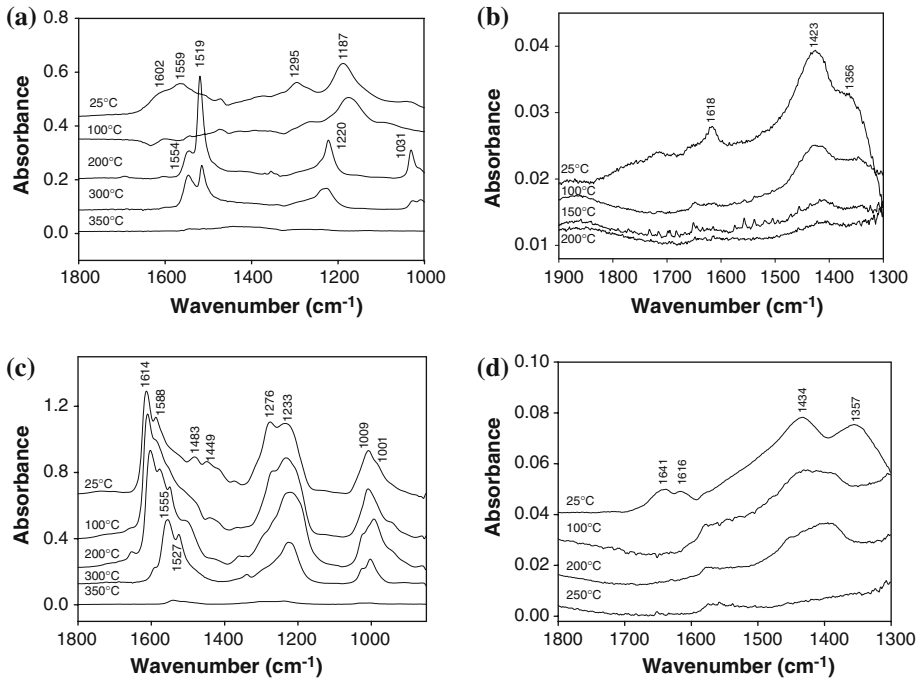

Figure 4. Evolution of DRIFT spectra in flowing Ar with increasing temperature after adsorbing (a) NO on Pt/CeO_2, (b) NO on Pt/SiO_2, (c) NO_2 on Pt/CeO_2 and (d) NO_2 on Pt/SiO_2.

and 1559 cm^{-1} indicate the presence of nitrates. Above 100 °C, significant changes in the spectrum were observed, suggesting the conversion of less stable forms of adsorbed NO into two main species. This is reflected in the spectrum recorded at 200 °C, containing two distinct bands at 1554 and 1519 cm^{-1} which can be assigned to two different types of nitrates, most likely monodentate [21,26–31]. The bands became narrow and proportionate with increasing temperature, until at 350 °C no observable NO_x species remained on the surface. These observations suggest that NO is adsorbed onto Pt/CeO_2 as a mixture of nitrite and nitrate species at room temperature, and that the nitrite reacts with lattice oxygen upon heating to afford nitrate. Similar results have been reported by Philipp *et al.* [22]: NO adsorption on CeO_2 at 50 °C was found to afford mainly nitrite and hyponitrite species ($N_2O_2^{2-}$), nitrate species being formed upon subsequent heating to 200 °C.

In comparison with Pt/CeO_2, Pt/SiO_2 exhibited much weaker bands upon adsorption of NO (figure 4(b)). A weak band at 1618 cm^{-1} can be assigned to NO adsorbed on Pt [32–34], although a bridging nitrate species cannot be excluded [26,27]. Bands at 1423 and 1356 cm^{-1} are probably due to NO adsorbed on SiO_2 in the form of nitrites [29,30,35]. All of these bands disappeared at 200 °C, indicating a much weaker interaction of NO with the Pt/SiO_2 surface than for Pt/CeO_2.

Analogous DRIFTS measurements were performed to characterize the surface species formed during NO_2 adsorption. As can be seen from figure 4(c), for Pt/CeO_2 the resulting IR bands are more intense than those obtained upon NO adsorption, suggesting a higher concentration of adsorbed species. At 25 °C bands were observed at 1614, 1588 and 1555 cm^{-1}, which are typical of bridging bidentate, chelating bidentate and monodentate nitrates, respectively. Nitrite species were also formed on the surface of Pt/CeO_2, as evidenced by bands at 1483 and 1449 cm^{-1}. Upon raising the temperature to 300 °C the bands became less intense and slightly narrower, consistent with partial desorption of the surface species. The residual species located at 1555 and 1527 cm^{-1} are ascribed to two different types of monodentate nitrates coexisting on the surface of Pt/CeO_2, as found for NO adsorption on Pt/CeO_2. Both of them can be completely removed by heating to 350 °C.

In the case of Pt/SiO_2, adsorption of NO_2 afforded spectra similar to those obtained with NO. At 25 °C weak bands were detected at 1641 and 1616 cm^{-1}, the former being assigned to NO_2 adsorbed on Pt, while the latter can again be assigned to either NO adsorbed on Pt (formed via NO_2 dissociation) or a bridging nitrate group on the support. Bands at 1434 and 1357 cm^{-1} again suggest the presence of nitrite groups. Raising the temperature to 100 °C resulted in the disappearance of the 1641 and 1616 cm^{-1} bands, and no adsorbed NO_x species of any kind remained at 250 °C.

3.2.2. *In situ DRIFTS study of NO oxidation*

As shown in figure 5, the spectra obtained for Pt/CeO_2 with flowing NO + O_2 at both 25 and 100 °C are very similar to the NO adsorption spectra at the corresponding temperatures. At 200 °C, two intense bands located at 1556 and 1528 cm^{-1} are observed, indicating that monodentate nitrates are the predominant surface species formed during NO oxidation. Above 300 °C, the bands at 1528, 1216, and 1030 cm^{-1} became weak, and at 400 °C the main surface species corresponded to the monodentate nitrate absorbing at 1556 cm^{-1}.

In situ DRIFT spectra of NO oxidation over Pt/SiO_2 are much simpler than those for Pt/CeO_2, the two main broad bands at 1419 and 1364 cm^{-1} observed upon exposure of the catalyst to NO and O_2 at 25 °C being very similar to the bands observed in the corresponding NO adsorption spectrum. Only one broad band at 1409 cm^{-1} was observed during the reaction at 200 °C, the intensity of which gradually decreased with increasing reaction temperature. Almost no species can be detected on the surface at 300 °C. The findings provide further evidence for the weak nature of the inter-

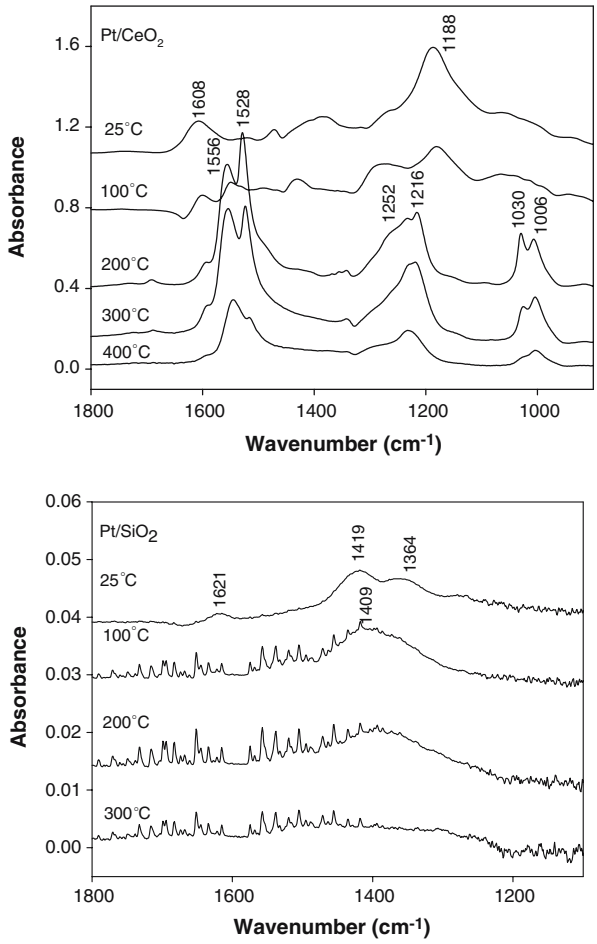

Figure 5. *In situ* DRIFT spectra of NO oxidation over Pt/CeO_2 and Pt/SiO_2. Feed: 500 ppm NO and 5.0% O_2 in Ar.

action of NO and NO_2 with the Pt/SiO_2 surface and are consistent with the mechanism suggested by Bernard *et al.* [5], in which NO weakly adsorbed on the silica support can undergo facile migration to Pt and subsequent reaction with adsorbed oxygen on Pt. The NO_2 product can either desorb directly from the Pt or migrate to the support. In the case of Pt/SiO_2, the low affinity of the silica support for NO_2 results in rapid NO_2 desorption, thereby freeing these sites for further adsorption of NO. This situation contrasts with Pt/CeO_2, on which NO_2 can remain strongly adsorbed as nitrate on the surface.

3.2.3. *Effect of SO_2*

In order to understand the origin of catalyst deactivation by SO_2 during NO oxidation, DRIFTS measurements were performed using a feed gas of NO and O_2 to which 20 ppm SO_2 was added. Figure 6 shows the DRIFTS spectra obtained at 300 °C with Pt/CeO_2 before and after addition of SO_2 to the feed. Upon adding SO_2, the intensity of the nitrate bands in the range 1600–1500 cm^{-1} decreased significantly, and additional bands formed in the range 1400–1300 cm^{-1} which remained after SO_2 addition was ceased (figure 6(c)). Subsequent treatment in flowing Ar at 400 °C resulted in the elimination of all nitrate species from the surface (disappearance of bands in the range 1600–1500 cm^{-1}), while bands located at 1400–1300, 1058 and 986 cm^{-1} indicated the presence of residual sulfur species. Based on previous studies [36,37], the bands between 1400 and 1300 cm^{-1} can be ascribed to sulfate formed on the surface of the ceria support, while the 986 cm^{-1} band corresponds to surface sulfite. These observations are consistent with the fact that metal sulfates are thermodynamically more stable than metal nitrates, with the consequence that prolonged exposure of metal oxides to SO_2 reduces their capacity to adsorb NO_x. Indeed, reactor studies show that after prolonged exposure to SO_2-containing NO/O_2 feed gas, Pt/CeO_2 is almost inactive for NO oxidation. Taken together, these observations reinforce the idea that NO adsorption onto the ceria support plays a key role in NO oxidation over Pt/CeO_2.

Analogous DRIFTS measurements performed for Pt/SiO_2 (figure 6(f)) show an increase in IR absorbance in the range 1400–1000 cm^{-1} after adding SO_2. The weak band at ~1150 cm^{-1} has a position similar to that of gaseous SO_2, suggesting that it may correspond to weakly bound SO_2 (i.e., physisorbed SO_2). Additionally, the formation of surface sulfate cannot be excluded due to the presence of very weak bands located in the sulfate range (> 1200 cm^{-1}). However, in contrast to Pt/CeO_2, the acidic nature of the silica surface clearly results in little adsorption of SO_2 or SO_3, while any adsorbed species are weakly bound. This accords with the finding that the activity of Pt/SiO_2 for NO oxidation is largely restored after removal of SO_2 from the feed.

3.2.4. *Effect of H_2O*

As presented in the kinetic study, the addition of H_2O to the feed resulted in the inhibition of NO oxidation over Pt/CeO_2, while no effect was observed for Pt/SiO_2. In an effort to clarify the origin of this inhibition, DRIFTS measurements were performed for Pt/CeO_2 with H_2O added to the feed. Figure 7 shows the result-

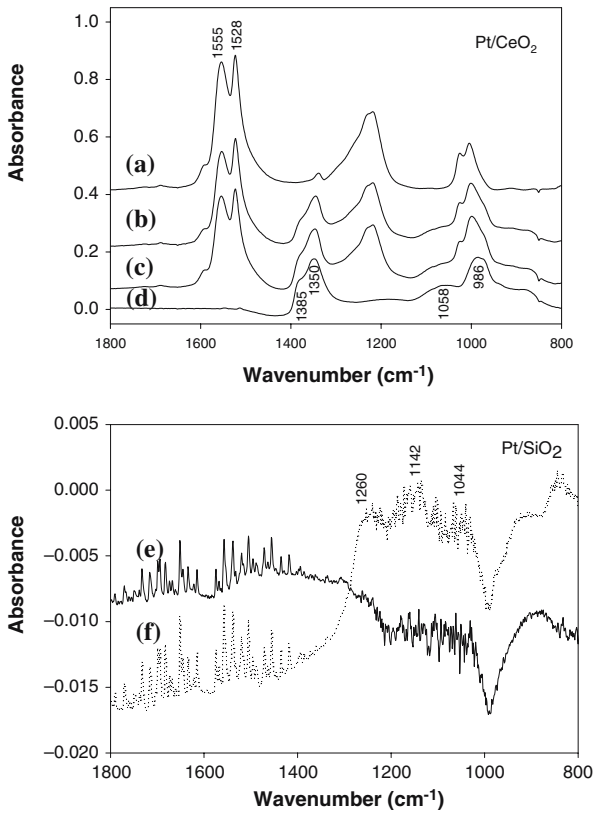

Figure 6. *In situ* DRIFT spectra of NO oxidation over Pt/CeO_2 and Pt/SiO_2 at 300 °C. Pt/CeO_2: (a) without SO_2 added; (b) with SO_2 added; (c) after turning off SO_2; and (d) after Ar purging at 400 °C. Pt/SiO_2: (e) without SO_2 added; (f) with SO_2 added.

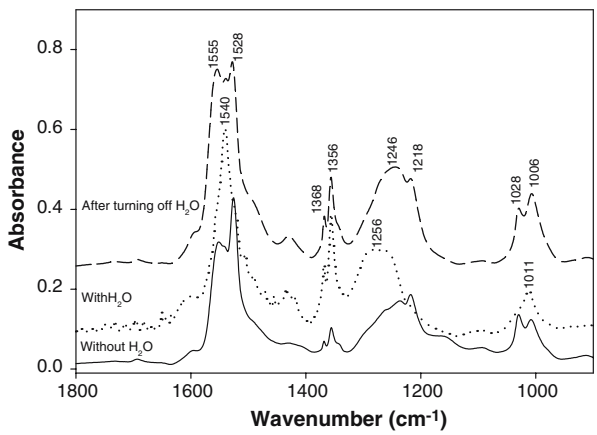

Figure 7. *In situ* DRIFT spectra of NO oxidation over Pt/CeO_2 at 200 °C (—) without H_2O in the feed, (.....) with H_2O, and (- - -) after turning off H_2O.

ing DRIFTS spectra. As discussed in Section 3.2.2, two types of nitrate, giving rise to bands at 1555 and 1528 cm^{-1}, are present on the surface during NO oxidation in the absence of H_2O. Upon the addition of H_2O, the three bands located at 1528, 1218 and 1028 cm^{-1} became weaker, while the bands located at 1555, 1246 and 1006 cm^{-1} were slightly enhanced. Simultaneously, a red shift of 15 cm^{-1} was observed for the band at 1555 cm^{-1}, together with a blue shift of 10 cm^{-1} for the band at 1246 cm^{-1}. Additionally, a growth of bands at 1368 and 1356 cm^{-1} was also observed, being assigned to two different types of surface nitrite [29,30,35]. An additional broad band was observed at 3560 cm^{-1}, which can be ascribed to hydroxyl groups formed on the ceria as a result of H_2O adsorption. Evidently, H_2O was competitively adsorbed with NO_x, with the consequence that the nitrate species absorbing at 1555 cm^{-1} is favored over the species absorbing at 1528 cm^{-1}. The observation of a red shift for the high-wavenumber band (1555 cm^{-1}) and a blue shift for the low-wavenumber band (1246 cm^{-1}) is consistent with a previous report that the adsorption of water reduces the splitting of the v_3 frequency of surface nitrate [30].

Upon ceasing the addition of H_2O to the feed there is a tendency to restore the original spectra, which correlates with the observation that catalyst activity can be fully recovered after a prolonged period of operation in the absence of H_2O. Overall these observations suggest that water is able to compete with NO_x for adsorption sites. Furthermore, it is apparent that the adsorption of H_2O not only reduces the number of the NO adsorption sites but also influences the nature of the adsorbed NO_x species.

4. Conclusions

Pt/CeO_2 possesses significant activity for NO oxidation, although it is less active than Pt/SiO_2. DRIFTS studies indicate that high concentrations of monodentate nitrate species exist on the surface of Pt/CeO_2 under the reaction conditions, while almost no surface species can be detected on Pt/SiO_2. Taken together these findings are consistent with a mechanism in which NO, weakly adsorbed on the silica support, migrates to Pt where it reacts with adsorbed oxygen. The NO_2 product can either desorb directly from the Pt or migrate to the support. In the case of Pt/SiO_2, the low affinity of the silica support for NO_2 results in rapid NO_2 desorption, thereby freeing these sites for further NO adsorption. This situation contrasts with Pt/CeO_2, on which NO_2 can remain strongly adsorbed as nitrate. Further, previous studies have shown that NO can adsorb on unpromoted ceria to form nitrate [21,22], i.e., the ceria itself can act as an oxidation catalyst. Given this fact, together with the highly oxidized state of the Pt in Pt/CeO_2 catalysts, it is likely that NO oxidation on Pt/CeO_2 involves oxygen spillover from Pt to the CeO_2 support (a process which has been well documented [38]), where NO oxidation occurs.

Pt/SiO_2 and Pt/CeO_2 also display contrasting behavior in the presence of SO_2. In the case of Pt/CeO_2, surface sulfates are formed at the expense of nitrate and nitrite species, the sulfates being stable to at least 400 °C. Consequently, poisoning of the catalyst is severe and irreversible below this temperature. For Pt/SiO_2 SO_x adsorption is weak and its influence is manifested as an inhibition of catalyst activity which largely disappears upon purging the catalyst at 300 °C. Pt particle sintering occurs as a result of exposure to SO_2, however, catalyst activity for Pt/SiO_2 is only slightly affected.

Acknowledgments

The authors thank Dr. Gerald Thomas for performing the XRF measurements, Mr. Dennis Sparks for experimental assistance, and Dr. Mark Keane for helpful discussions. This publication was prepared with the support of the U.S. Department of Energy, under Awards No. DE-FG26-04NT42197 and DE-FC26-05NT42631. However, any opinions, findings, conclusions, or recommendations expressed herein are those of the authors and do not necessarily reflect the views of the DOE.

References

[1] W.S. Epling, L.E. Campbell, A. Yezerets, N.W. Currier and J.E. Parks II, Catal. Rev. 46 (2004) 163.
[2] J. Gieshoff, A. Schäfer-Sindlinger, P.C. Spurk, J.A.A. van den Tillaart and G. Garr, Society of Automotive Engineers, 2000-01-0189 (2000).
[3] B.A.A.L. van Setten, M. Makkee and J.A. Moulijn, Catal. Rev. Sci. Eng. 43 (2001) 489.
[4] E. Xue, K. Seshan and J.R.H. Ross, Appl. Catal. B: Environ. 11 (1996) 65.
[5] S. Bernard, L. Retailleau, F. Gaillard, P. Vernoux and A. Giroir-Fendler, Appl. Catal. B: Environ. 55 (2005) 11.
[6] J. Oi-Uchisawa, A. Obuchi, R. Enomoto, S. Liu, T. Nanba and S. Kushiyama, Appl. Catal. B: Environ. 26 (2000) 17.
[7] P. Denton, A. Giroir-Fendler, H. Praliaud and M. Primet, J. Catal. 189 (2000) 410.
[8] J.-H. Lee and H.H. Kung, Catal. Lett. 51 (1998) 1.
[9] L. Olsson and E. Fridell, J. Catal. 210 (2002) 340.
[10] S.S. Mulla, N. Chen, W.N. Delgass, W.S. Epling and F.H. Ribeiro, Catal. Lett. 100 (2005) 267.
[11] M. Crocoll, S. Kureti and W. Weisweiler, J. Catal. 229 (2005) 480.
[12] L. Olsson, H. Persson, E. Fridell, M. Skoglundh and B. Andersson, J. Phys. Chem. B 105 (2001) 6895.
[13] L. Olsson, B. Westerberg, H. Persson, E. Fridell, M. Skoglundh and B. Andersson, J. Phys. Chem. B 103 (1999) 10433.
[14] R. Burch and T.C. Watling, J. Catal. 169 (1997) 45.
[15] J. Després, M. Elsener, M. Koebel, O. Kröcher, B. Schnyder and A. Wokaun, Appl. Catal. B: Environ. 50 (2004) 73.
[16] F. Jayat, C. Lembacher, U. Schubert and J.A. Martens, Appl. Catal. B: Environ. 21 (1999) 221.
[17] R. Marques, P. Darcy, P. Da Costa, H. Mellottée, J.-M. Trichard and G. Djéga-Mariadassou, J. Mol. Catal. A: Chem. 221 (2004) 127.

[18] K.E. Voss, S. Roth, J.C. Dettling, G.W. Rice, Y.K. Lui and M. Yassine, PCT Int. Appl. WO 2000029726 (2000).
[19] F. Rohr, S.D. Peter, E. Lox, M. Kögel, A. Sassi, L. Juste, C. Rigaudeau, G. Belot, P. Gélin and M. Primet, Appl. Catal. B: Environ. 56 (2005) 201.
[20] J. Theis, J. Ura, C. Goralski Jr., H. Jen, E. Thanasiu, Y. Graves, A. Takami, H. Yamada and S. Miyoshi, Society of Automotive Engineers, 2003-01-1160 (2003).
[21] M. Haneda, T. Morita, Y. Nagao, Y. Kintaichi and H. Hamada, Phys. Chem. Chem. Phys. 3 (2001) 4696.
[22] S. Philipp, A. Drochner, J. Kunert, H. Vogel, J. Theis and E.S. Lox, Topics Catal. 30–31 (2004) 235.
[23] Y. Ji, D. Sparks, A. Tackett and M. Crocker, Fuel, submitted.
[24] J.R. Chang, S.L. Chang and T.B. Lin, J. Catal. 169 (1997) 338.
[25] A.F. Lee, K. Wilson, R.M. Lambert, C.P. Hubbard, R.G. Hurley, R.W. McCabe and H.S. Gandhi, J. Catal. 184 (1999) 491.
[26] T. Toops, D. Smith, W. Epling, J. Parks and W. Partridge, Appl. Catal. B: Environ. 58 (2005) 255.
[27] K. Shimizu, H. Kawabata, A. Satsuma and T. Hattori, J. Phys.Chem. B. 103 (1999) 5240.
[28] C. Sedlmair, K. Seshan, A. Jentys and J. Lercher, J. Catal. 214 (2003) 308.
[29] F. Meunier, V. Zuzaniuk, J. Breen, M. Olsson and J. Ross, Catal. Today 59 (2000) 287.
[30] D. Pozdnyakov and V. Fillmonov, Kinet. Catal. 14 (1973) 655.
[31] H. Huang, R. Long and R. Yang, Energy Fuels 15 (2001) 205.
[32] A. Bourane, O. Dulaurent, S. Salasc, C. Sarda, C. Bouly and D. Bianchi, J. Catal. 204 (2001) 77.
[33] P. Levy, V. Pitchon, V. Perrichon, M. Primet, M. Chevrier and C. Gauthier, J. Catal. 178 (1998) 363.
[34] R. van Slooten and B. Nieuwenhuys, J. Catal. 122 (1990) 429.
[35] W.S. Kijlstra, D.S. Brands, E.K. Poels and A. Bliek, J. Catal. 171 (1997) 208.
[36] P. Bazin, O. Saur, J. Lavalley, G. Blanchard, V. Visciglio and O. Touret, Appl. Catal. B: Environ. 13 (1997) 265.
[37] M. Waqif, P. Bazin, O. Saur, J. Lavalley, G. Blanchard and O. Touret, Appl. Catal.B: Environ. 11 (1997) 193.
[38] A. Galdikas, C. Descorme and D. Duprez, Solid State Ionics 166 (2004) 147.